FEBS 26840 FEBS Letters 533 (2003) 47–53

Pre-transmembrane sequence of Ebola glycoprotein. Interfacial hydrophobicity distribution and interaction with membranes

Asier Sáez-Cirión[1], María J. Gómara, Aitziber Agirre, José L. Nieva*

Unidad de Biofísica (CSIC-UPV/EHU) and Departamento de Bioquímica, Universidad del País Vasco, Aptdo. 644, 48080 Bilbao, Spain

Received 26 September 2002; accepted 13 November 2002

First published online 2 December 2002

Edited by Irmgard Sinnig

Abstract **The membrane-interacting domain that precedes the transmembrane anchor of Ebola glycoprotein has been characterized. This aromatic-rich region is predicted to bind the membrane interface adopting an α-helical structure. Peptides representing either the Ebola glycoprotein pre-transmembrane sequence, or a 'scrambled' control with a different hydrophobic-at-interface moment, have been studied. Insertion into lipid monolayers, changes in intrinsic fluorescence and in infrared spectra demonstrated that only the wild-type peptide bound the interface under equilibrium conditions and adopted an α-helical conformation. The presence of the raft-associated lipid sphingomyelin did not affect membrane insertion, but it stimulated highly the membrane-destabilizing capacity of the pre-transmembrane sequence. A parallel study of the effects of the viral sequence and of melittin suggests that Ebola glycoprotein pre-transmembrane sequence might target membranes inherently prone to destabilization by lytic peptides.**

Key words: Viral fusion protein; Interfacial hydrophobicity; Protein–lipid interaction; Infrared spectroscopy; Ebola GP2

1. Introduction

Ebola virus glycoprotein (GP) is responsible for both receptor binding and membrane fusion during viral entry into the host cells [1,2]. This glycoprotein is synthesized as a precursor molecule and subsequently cleaved by furin into two disulfide-linked subunits, surface (GP1) and transmembrane (GP2) [1,2]. The crystal structure of GP2 ectodomain has been determined and consists of a trimeric helical bundle whose core is organized as a triple-stranded coiled-coil [3,4]. The coiled-coil structure plays an important role in facilitating the entry of Ebola virus into host cells [5]. It has been recently demonstrated that GP associates with lipid rafts after synthesis, suggesting that Ebola might assemble and emerge through these distinct lipid microdomains [6]. In the same work, evidence is also provided in support of the idea that rafts play a critical role at the entry stage of Ebola infection.

Mutagenesis and biophysical characterization confirmed earlier predictions indicating the existence in GP2 of an internal fusion peptide consisting of approximately 16 uncharged hydrophobic residues [7–9]. Ebola GP also contains within the membrane-proximal region of the GP2 ectodomain a second sequence showing a high tendency to partition into membrane interfaces [10,11]. Computation of the hydrophobic-at-interface moment for this element reflects a tendency to segregate interfacial residues into a defined surface of an α-helix, suggesting that the GP2 pre-transmembrane sequence (preTM) might partition into membranes adopting a helical structure. Experimental work demonstrated that the sequence fulfills the predictions of the Wimley–White [12] algorithms, namely spontaneous partitioning into membrane interfaces and an α-helix representing the main conformation of the soluble and membrane-inserted forms. Disturbance of the helical moment by scrambling the sequence interfered with its ability to fold in solution and in membranes adopting a helical structure, as well as with the partitioning equilibrium. Wild-type Ebola pre-TM, but not scrambled Ebola pre-TM, breached the permeability barrier of membranes. Of note, permeabilization was promoted in the presence of sphingomyelin (SM), a raft-associated lipid. Our results sustain the notion that the aromatic-rich pre-transmembrane domain in Ebola glycoprotein may interact monotopically with membranes as an α-helix and promote perturbations therein. The findings in this work may help in understanding the molecular mechanism by which Ebola GP2 induces membrane merging.

2. Materials and methods

Cholesterol (CHOL), egg phosphatidylcholine (PC), egg phosphatidylethanolamine (PE), and brain SM were purchased from Avanti Polar Lipids (Birmingham, AL, USA). 8-Aminonaphthalene-1,3,6-trisulfonic acid sodium salt (ANTS) and *p*-xylenebis(pyridinium)bromide (DPX) were from Molecular Probes (Junction City, OR, USA). D_2O, *N*-acetyl-L-tryptophanamide and Triton X-100 were obtained from Sigma (St. Louis, MO, USA). All other reagents were of analytical grade. The sequences representing the pre-transmembrane stretch of Ebola GP2 (residues 640–657 of Ebola GP precursor, Zaire strain, GenBank U31033), DNDNWWTGWRQWIPAGIG (EBO_c) and its scrambled variant DWGDAPNWRWNWGIIGTQ (EBO_{scr}) were synthesized as C-terminal carboxamides and purified (estimated homogeneity >90%) by Neosystem (Strasbourg, France). Synthetic melittin was obtained from Bachem (Bubendorf, Switzerland). Peptide stock solutions were prepared in dimethylsulfoxide (spectroscopy grade).

To compute the hydrophobic-at-interface moment, we considered

*Corresponding author. Fax: (34)-94-464 8500.
E-mail address: gbpniesj@lg.ehu.es (J.L. Nieva).

[1] Present address: Center for Biologics Evaluation and Research, Food and Drug Administration, Bethesda, MD 20892, USA.

Abbreviations: ANTS, 8-aminonaphthalene-1,3,6-trisulfonic acid; CHOL, cholesterol; DPX, *p*-xylenebis(pyridinium)bromide; IR, infrared spectroscopy; EBO_c, synthetic sequence (20 aa) representing residues 640–657 of Ebola GP precursor (Zaire strain, GenBank accession no. U31033); EBO_{scr}, scrambled EBO_c; LUV, large unilamellar vesicles; PC, phosphatidylcholine; PE, phosphatidylethanolamine; SM, sphingomyelin

0014-5793/02/$22.00 © 2002 Published by Elsevier Science B.V. on behalf of the Federation of European Biochemical Societies.
PII: S0014-5793(02)03747-X

the membrane interface-to-water transfer free energies (ΔG_{iwu}) for each amino acid [12] as the moduli of the vectors that project from the main axes of the secondary structure element, following the direction of the amino acid side chains [13]. The hydrophobic moment (μ_{H}) of a sequence of N residues was then calculated as the addition of the N hydrophobicity vectors corresponding to the constituent amino acids, following the equation [13,14]:

$$\mu_{\mathrm{H}} = \left(\left(\sum_{n=1}^{N} H_n \sin(\delta n) \right)^2 + \left(\sum_{n=1}^{N} H_n \cos(\delta n) \right)^2 \right)^{1/2}$$

where H_n is the hydrophobicity of the n residue, and δ is the angle formed between side chains of consecutive residues, i.e. 100° for helical conformations.

Large unilamellar vesicles (LUV) were prepared according to the extrusion method of Hope et al. [15] in 5 mM HEPES, 100 mM NaCl (pH 7.4). When required, osmolalities were adjusted to 200 mOsm in a cryoscopic osmometer (Osmomat 030, Gonotec, Berlin, Germany). Lipid concentrations of liposome suspensions were determined by phosphate analysis [16]. The average diameter of vesicles was ca. 100 nm according to quasi-elastic light scattering determinations using a Malvern Zeta-Sizer instrument.

For assays of monolayer penetration [17] surface pressure was determined in a fixed-area circular through (μTrough S system, Kibron, Helsinki, Finland). Measurements were carried out at room temperature and under constant stirring. The aqueous phase consisted of 1 ml 5 mM HEPES, 100 mM NaCl (pH 7.4). Lipids, dissolved in chloroform, were spread over the surface and the desired initial surface pressure (π_0) was attained by changing the amount of lipid applied to the air–water interface. Peptide was injected into the subphase with a Hamilton microsyringe. At the concentrations used the peptide alone induced a negligible increase in surface pressure at the air–water interface.

Peptide insertion into bilayers was subsequently evaluated by monitoring the change in emitted Trp-fluorescence upon partitioning into LUV [18]. Corrected spectra were obtained in a Perkin Elmer MPF-66 spectrofluorimeter with the excitation set at 280 nm and 5-nm slits. In selected instances partitioning curves were subsequently computed from the fractional change in emitted Trp-fluorescence when titrated with increasing lipid concentrations, as described in [18].

Release of vesicular contents or leakage to the medium was monitored by the ANTS/DPX assay [19]. The procedure is described in detail in [20]. All these fluorescence measurements were conducted in thermostatically controlled cuvettes (25°C). The medium in the cuvettes was continuously stirred to allow the rapid mixing of peptide and vesicles.

Infrared spectroscopy (IR) measurements were conducted essentially as in [20]. Samples in the presence of vesicles consisted of floated peptide–lipid complexes obtained in D_2O buffer after ultracentrifugation. Solvent samples were also obtained from the supernatant fraction not containing lipid or peptide and subsequently used as background controls. Infrared spectra were recorded in a Nicolet 520 spectrometer equipped with an MCT detector. Samples were placed between two CaF_2 windows separated by 50-μm spacers. 1000 scans (sample) and 1000 scans (reference) were taken for each spectrum, using a shuttle device. Subtraction and band position determination were performed according to procedures described in [21] with the help of OMNIC and Grams softwares.

3. Results and discussion

3.1. Description of Ebola GP pre-transmembrane as an interfacial sequence

Fig. 1A shows the membrane-partitioning sequences within Ebola GP. The plot in this figure is based on the hydrophobicity-at-interface scale as determined by Wimley and White [12]. The sequence at the N-terminus of the GP1 subunit, SP, corresponds to the signal peptide. The internal fusion peptide FP is located close to the GP2 N-terminus. This stretch comprises approximately residues 524GAAIGLAWIPYFGPAA539 [7–9]. An additional conspicuous region (marked preTM in Fig. 1A) showing affinity for membrane interfaces spans

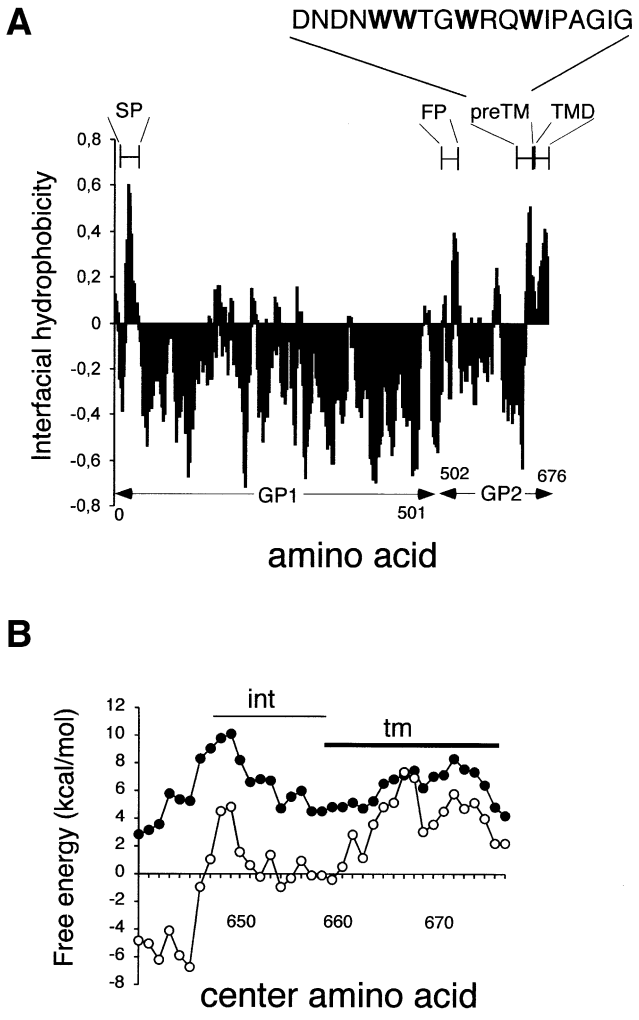

Fig. 1. A: Interfacial hydrophobicity of the surface Ebola GP precursor (Zaire strain, GenBank accession number: U31033). The plot (mean values of free energies of transfer from membrane interfaces to water for a window of 11 amino acids) was constructed using the Wimley–White scale for individual residues [12]. Designated regions include: SP, signal peptide; FP, fusion peptide; preTM, pre-transmembrane; TMD, transmembrane domain. B: Standard free energies of transfer (kcal mol^{-1}) from octanol (○) and interface (●) to water for the preTM/TMD region of Ebola GP (residues 640–676, i.e. last 37 residues). Plots represent for each center amino acid the sum of free energies in windows of 11 residues. Interfacial values include conformational free energy contribution (see text for details). Horizontal lines indicate the predicted locations for the transmembrane (tm) and interfacial helices (int).

approximately residues 640DNDNWWTGWRQWIPAGIG-657, preceding the C-terminal hydrophobic 658–676 transmembrane (TMD) anchor. Apart from FP, preTM and TMD, no other relevant membrane-interacting regions are found in the mature Ebola glycoprotein.

With the aim of comparing bilayer partitioning with bulk-phase partitioning, Wimley and White also established a whole-residue hydrophobicity scale for partitioning into *n*-octanol [10–12]. The octanol scale provides a reasonable estimate of the free energy of inserting α-helical amino acid residues into bilayers, i.e. it results particularly suitable to distinguish TMDs in hydropathy plots [22]. Thus we analyzed in more detail the putative low-energy membrane organization of the preTM/TMD region in Fig. 1B. Hydropathy was ini-

tially computed using the octanol-to-water partitioning free energies (empty circles), i.e. positive values in the plot denote tendency to remain in the octanol phase. The plot reveals the existence of a stretch (int), close to the 0 equilibrium value, which is followed by a region with a transmembrane tendency (tm). Hydropathy was complementarily estimated as interfacial partitioning. To make both partitioning processes comparable, the conformational energy, approximately −0.41 kcal mol^{-1} per residue adopting an α-helical conformation [23], must be added to the free energy of partitioning into interfaces of the unfolded sequence (see [24] for detailed explanations). In Fig. 1B we include a plot (filled symbols) which is based on the membrane interface:water free energy of partitioning, including conformational energy (i.e. positive values in this case denote a tendency to remain interface-bound). When compared to the octanol plot, the interfacial plot displayed more positive values within the 'int' segment, indicating the higher preference of this region for the interface. In contrast, the 'tm' region displayed rather similar values in both plots, a fact compatible with the theoretical existence of the TMD stretch in equilibrium between the octanol and membrane interface phases. In summary, hydropathy data in Fig. 1 are consistent with the existence in the carboxy-end of GP2 of an interfacial-transmembrane structural motif.

Membrane interaction of Ebola GP preTM was further characterized with the hydrophobic-at-interface moment (Fig. 2). This analysis revealed that the sequence would generate one face with a strong affinity for membranes if folded as an α-helix (Fig. 2A). Hydrophobic moments measure the periodicity of residue distribution along the secondary structure elements [13,14]. Orienting hydrophobic residues preferentially towards one face of the element has been proposed to favor hydrophobic interactions between membranes and protein sequences. The moment, calculated as a function of the angle between consecutive residues (δ), displayed for GP preTM a maximum at about $\delta = 100°$, indicating that adoption of an α-helical conformation in solution optimizes the residue distribution required for effective partitioning into membrane interfaces (Fig. 2A).

The hydrophobic moment plots with fixed $\delta = 100°$ corresponding to GP preTM/TMD sequences derived from the different Ebola subtypes and Marburg (Musoke strain) detected a peak just preceding the transmembrane anchor (Fig. 2B). The alignment of these carboxy-terminal GP sequences confirms a high degree of conservation of interfacial Trp and Leu residues within the preTM region (data not shown). Thus, the presence of an amphipathic interfacial helix located at the membrane-proximal region of GP seems to be a common structural motif among members belonging to the *Filoviridae* family. Experimental evidence is provided below suggesting that this GP structural element is able to sustain an interaction with membranes.

3.2. GP preTM interactions with membranes

The membrane-interacting ability of EBO_c, a peptide representing the preTM of Ebola GP (Zaire strains), was initially assessed. A scrambled sequence of the same region, EBO_{scr}, was designed as a negative control. This control sequence displayed a hydrophobic-at-interface moment maximum shifted to $\delta = 180°$ (see Fig. 2A), and therefore it was predicted to adopt non-helical, amphipathic extended structures in contact with membrane interfaces. EBO_c and EBO_{scr} penetration

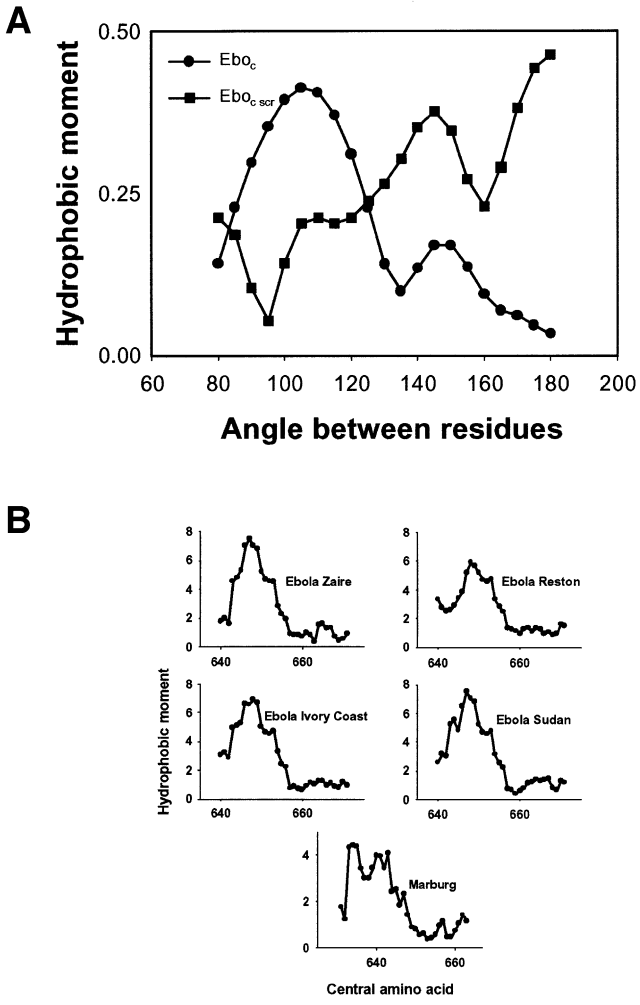

Fig. 2. A: Hydrophobic-at-interface moment of the 640–657 Ebola GP (Zaire subtypes) segment (●) and a scrambled sequence (■), calculated as a function of the δ angle. B: Hydrophobic-at-interface moments for a fixed $\delta = 100°$ corresponding to similar regions derived from the different filoviruses indicated in the panels. Represented values are the sum of the moments in a window of length 11 amino acids, or approximately three helical turns.

into membranes was first studied by the monolayer technique (Fig. 3A). We anticipated that, being predicted to be interfacial sequences, these peptides might partition into lipid monolayers altering their surface pressure. The penetration capacity depending on the lipid film initial pressure (π_0) was determined measuring the monolayer exclusion pressure (π_{ex}), i.e., the π_0 at which no increment in pressure ($\Delta\pi = 0$) was observed afer peptide injection into the subphase [17]. The π_{ex} values obtained from plots in Fig. 3A were 33.0 mN m^{-1} and 31.5 mN m^{-1} for EBO_c and EBO_{scr}, respectively, indicating a comparable capacity of both sequences to penetrate into membranes. Moreover, both values lie within the range of lateral pressures expected in biological membranes ($\pi_0 \geq 30$–35 mN m^{-1} [25]).

Fig. 3B,C shows data on the capacity of EBO_c and EBO_{scr} to partition and insert into vesicle membranes. Spectra in Fig. 3B demonstrate that EBO_c intrinsic fluorescence increased and shifted the maximum emission wavelength (from 354 to 340 nm) in the presence of PC LUV. This is indicative of the Trp residues sensing a low-polarity environment provided by

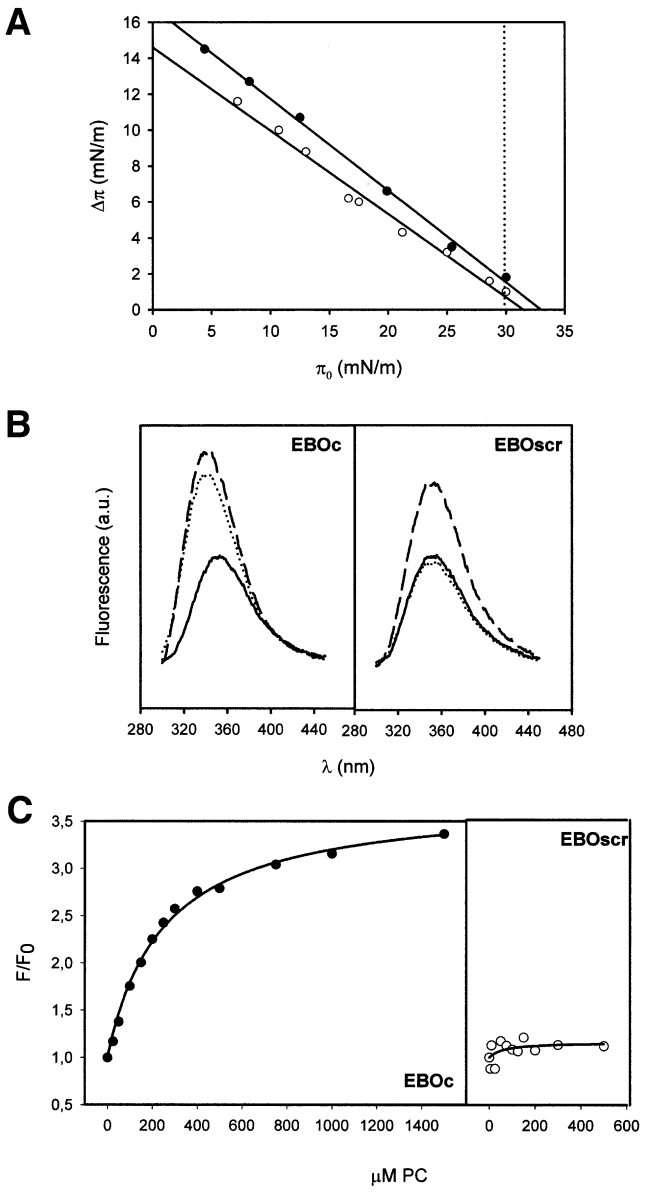

Fig. 3. A: Penetration of EBO_c (filled symbols) and EBO_{scr} (empty symbols) into PC monolayers. Maximum increase in surface pressure induced upon injection of 0.23 μM peptide in the subphase was measured as a function of the initial surface pressure of the phospholipid monolayers. B: Fluorescence emission spectra of EBO_c and EBO_{scr}. Solid lines: peptide in buffer; Discontinuous lines: peptides added to PC LUV; Dotted lines: peptides pre-incubated in solution (15 min) before addition of vesicles. Peptide concentration was 0.5 μM and, in vesicle samples, the peptide-to-lipid mole ratio was 1:200. C: Partitioning curves as estimated from the fractional change in Trp fluorescence in the presence of increasing amounts of PC LUV. The solid lines correspond to the best fittings of the experimental values to a hyperbolic function. Symbols as in panel A.

the bilayer. EBO_{scr} intrinsic fluorescence also increased but the position of the emission maximum did not change when added to vesicles. A more significant difference could be observed when peptides were pre-incubated in solution before vesicle addition. EBO_c fluorescence again increased and blue-shifted, indicating that pre-incubation in solution did not affect the partitioning equilibrium of this peptide. In contrast, EBO_{scr} emission did not appreciably change upon addition of vesicles indicating that the peptide lost the capability to partition into membranes under these conditions. It appears that effective incorporation of EBO_{scr} into membranes could only be achieved under non-equilibrium conditions, i.e. most likely before a competing self-aggregation process evolved. This is further illustrated by the fractional change in peptide intrinsic fluorescence upon titration with increasing amounts of lipid vesicles (Fig. 3C). While EBO_c Trp emission increased and reached saturation, EBO_{scr} fluorescence did not change significantly. Thus, in contrast with the peptide representing the functional sequence, incubation of EBO_{scr} in solution led to self-aggregation, a possibility that was supported by the IR experiments (see below).

IR data in Fig. 4 are consistent with different conformations being adopted by EBO_c and EBO_{scr} in solution and associated to membranes. The conformation sensitive amide I band of EBO_c in deuterated buffer (Fig. 4A) showed a main component at 1647 cm^{-1}. In this region the presence of unordered structures has been described ($\sim$1643 cm^{-1}) together with absorption by α-helical conformations (1641–1658 cm^{-1}) [21]. In contrast, maximum absorption by the EBO_{scr} peptide was found at 1619 cm^{-1}, a band related to intermolecular interaction of β-like extended conformations, such as those found for amyloid-type aggregates. This is confirmed by the simultaneous presence of a minor component at high-field ($\sim$1680 cm^{-1}) described for this type of extended structures.

The spectra in Fig. 4B were obtained in the presence of PC LUV. In EBO_c samples, within the amide I region appeared a conspicuous band centered at 1647 cm^{-1} which indicates that the preferential structure adopted by the peptide in membranes was also α-helical. To study the structure of EBO_{scr} in membranes, the peptide was added to vesicles already present in solution. The spectrum of EBO_{scr} associated to membranes reflects that lipids did not change the main conformation adopted by the peptide either, but in this case the low-field band was split into two sharper components centered at 1629 and 1615 cm^{-1}. These bands may be assigned to classical antiparallel β-sheets and intermolecularly H-bonded aggregates of extended structure, respectively [21].

In summary, from the IR data above it may be deduced that the sequence representing the functional pre-transmembrane region of Ebola GP adopts an α-helical conformation both in solution and in membranes. Preservation of the hydrophobicity-at-interface distribution within this helical structure appears to be required for efficient partitioning and folding into membranes. Thus, the preTM is not merely a cluster of aromatic residues showing a tendency to interact with membranes, but it also adopts an intrinsic structure that optimizes partitioning into membrane interfaces.

These results may be further discussed in the context of current understanding of the energetics of interfacial partitioning [22,24]. The fraction of helical content of membrane-bound EBO_c was ca. 0.8 as estimated from IR data (Fig. 4B), which corresponds to approximately 13–14 residues adopting a defined helical conformation. Thus, considering a per-residue change of −0.41 kcal mol^{-1} [23], the free energy change upon peptide folding at interfaces (ΔG_{if}) would amount to (−5.3)–(−5.7) kcal mol^{-1}. The partitioning isotherm displayed in Fig. 3C rendered an experimental K_x value of 2.2×10^5 for EBO_c partitioning into PC LUV. Computation of the maximum total free energy of partitioning ($\Delta G_t = -RT\times\ln K_x$) gives an estimate of ca. −7.3 kcal

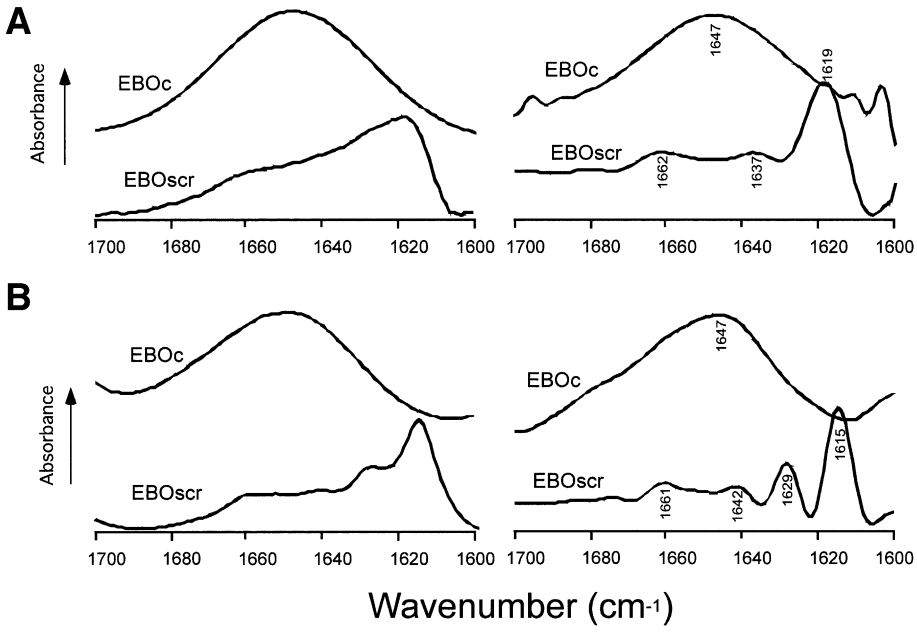

Fig. 4. Infrared spectra of EBO_c and EBO_{scr}, in the amide I region. A: IR spectra in D_2O buffer. B: IR spectra of peptides associated to PC vesicles. Peptide and vesicles were incubated at a peptide-to-lipid ratio of 1:20, peptide bound to vesicles was subsequently isolated by flotation in D_2O buffer as previously described [20]. Right-hand panels correspond to Fourier-deconvolved spectra.

mol^{-1}. In consequence, conformational free energy appears to be the main contribution to EBO_c interfacial partitioning. Interfering with the ability of the Ebola preTM sequence to fold correctly as an α-helix by redistributing interfacial residues, results in low membrane partitioning at equilibrium and formation of intermolecularly H-bonded extended strands, both in solution and at interfaces.

The experimental results in Table 1 summarize the effects of different lipid compositions on peptide bilayer penetration and efflux. Comparable shifts of EBO_c fluorescence emission maximum towards shorter wavelengths could be detected in the presence of vesicles made of different lipid compositions. This fact confirms that penetration occurred in all the mixtures tested. However, leakage was barely detectable in vesicles devoid of the raft-associated lipid SM [26–28]. The presence of SM at increasing molar fractions promoted the peptide permeabilizing effect. Moreover, heating PC:SM mixtures above the transition temperature of SM ($T_c \sim 39°C$) inhibited leakage induced by the peptide but not its penetration. These observations are consistent with a SM effect stemming from its ability to laterally segregate into ordered lipid phases [26–28]. It should be pointed out that efflux induced by EBO_c was not accompanied by vesicle aggregation or fusion (data not shown). Thus membrane perturbations leading to the observed permeabilization occurred within isolated vesicles.

The SM effect seemed to not arise from an intrinsic instability of these vesicles, since the control EBO_{scr} sequence could not induce leakage at any tested dose even though it interacted with liposomes (see lipid-induced structural changes in EBO_{scr}, Fig. 4). This result underscores the importance of residue distribution within the preTM sequence for the induction of membrane perturbations. However, since EBO_{scr} peptide does not interact with membranes in a reproducible manner under equilibrium conditions (Fig. 3), we used melittin as a control to explore in more detail the specific role of SM (Fig. 5). Melittin, the main proteinaceous component of honeybee venom, has been extensively studied as a model peptide for lytic peptide–lipid interactions ([29–31], and references therein). In particular, melittin has been shown to locate at the interface of electrically neutral PC membranes as a helical monomer [32] and induce dose-dependent permeabilization of PC vesicles [29–31]. In agreement with previously reported data [29], melittin-induced efflux of PC vesicle contents was already observed at a peptide-to-lipid mole ratio of 1:1000, while maximum permeabilization levels were attained at 1:100 (Fig. 5A). Unexpectedly, inclusion of 50 mol% SM into the lipid vesicle composition decreased these peptide-to-lipid mole ratios by an order of magnitude. Although EBO_c required higher peptide-to-lipid mole ratios than melittin to induce

Table 1
Interactions of EBO_c with model membranes. Influence of lipid composition on intrinsic fluorescence and induction of leakage

	Δλ (nm)[a]	Leakage (%)[b]
PC	−14	10
PC[c]	0	< 5
PC[d]	−18	12
PC:SM (2:1)	−13	38
PC:SM (1:1)	−13	83
PC:SM (1:1)[c]	0	< 5
PC:SM (1:1)[d]	−18	98
PC:SM (2:1) $T = 50°C$	−10	8
PC:SM (1:1) $T = 50°C$	−10	< 5
PC:CHOL (2:1)	−10	8
PC:CHOL (1:1)	nd	< 5
PC:SM:CHOL (1:1:1)	−10	20
PC:PE:SM:CHOL (1:1:1:1.5)	−9	< 5

[a]Increase in Trp maximum emission wavelenght. Maximum emission wavelength of the peptides (0.5 μM) in buffer was 354 nm. Peptide-to-lipid ratio was 1:200.
[b]Percentage of leakage measured at time = 30 min. The peptide-to-lipid mole ratio was 1:20 and the lipid concentration 100 μM.
[c]Measurements were carried out using the EBO_{scr} control sequence.
[d]Measurements were carried out using melittin as a control. Leakage was measured at a peptide-to-lipid mole ratio of 1:1000.

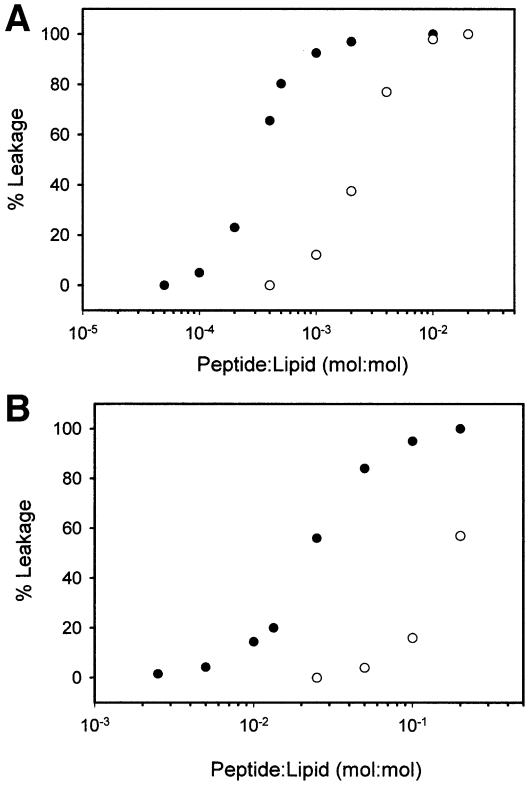

Fig. 5. Peptide-induced ANTS/DPX efflux from LUV. Melittin (A) and EBO_c (B) were added at various concentrations to vesicles composed of PC (open symbols) and PC:SM (1:1 mole ratio) (closed symbols). Extents of released probe were monitored 30 min after peptide addition. Lipid concentration in each sample was 100 μM.

leakage of vesicles (Fig. 5B), the stimulatory effect of the SM lipid seemed to be similar to that observed for melittin. As for the case of EBO_c, we observed comparable shifts in fluorescence emission maximum of melittin Trp towards shorter wavelengths with increasing amounts of PC and PC:SM (1:1) vesicles (see Table 1), a fact consistent with a similar degree of association to both membranes. To our knowledge this stimulatory effect of SM on the capacity of melittin to permeabilize vesicles was not previously described. We note here that melittin permeabilized SM-containing vesicles at peptide-to-lipid mole ratios, i.e. 1:10 000, far below those required for induction of macroscopic changes (disc formation) which occur at peptide-to-lipid mole ratios as high as 1:10 [33].

3.3. Concluding remarks

Our study combining a new predictive tool with experimental verification suggests that the preTM sequence of Ebola GP is a membrane-partitioning helical domain with an ability to perturb the integrity of SM-containing phospholipid bilayers. Thus, the preTM sequence would immerse into the SM-rich viral membrane milieu that seems to be inherently more prone to destabilization by a membrane-disrupting toxic peptide such as melittin. One can speculate that lipid modulation of the ability to break down the membrane permeability barrier is a common adaptive mechanism among sequences of diverse origin. Melittin shows high hemolytic activity and membrane specificity for zwitterionic phospholipids in vesicle leakage assays [29–31]. SM is abundant at the external monolayer of the erythrocyte and other cell plasma membranes, therefore it would be a good candidate to modulate the toxic action of melittin. Ebola GP preTM sequence might use similar mechanisms to damage the membrane organization of the viral envelope.

Thus, the preTM may constitute a functional element of Ebola GP implied in the promotion of the membrane destabilization required for fusion. It has been hypothesized that the helical core structure of GP2 subunit would bring the two hydrophobic regions not appearing in the crystal, FP and preTM/TMD, to close spatial proximity [3,4]. The GP2 preTM sequence might in this way play an active role in perturbing apposed membranes during fusion. Detection and characterization of functional sequences within the fusion mediator GP are crucial since they might become in the future putative targets for specific anti-Ebola therapeutics. We have recently shown that an equivalent preTM region in fusogenic gp41 HIV-1 associates with raft-type lipids and induces membrane perturbations [34]. This HIV-1 region seems to be recognized by anti-gp41 broadly neutralizing monoclonal antibodies and has been proposed to represent an important focus for clinical intervention [35]. In this sense, the Ebola GP preTM might also represent an attractive focus for the development of antiviral strategies.

Acknowledgements: We thank F.M. Goñi and G. Basañez for their critical reading of the manuscript. This work was supported by DGCYT (BIO2000-0929), the Basque Government (EX-1998-28; PI-1998-32) and the University of the Basque Country (UPV 042.310-EA085/97; UPV 042.310-G03/98). A.S.-C. and A.A. were recipients of predoctoral fellowships of the Basque Government.

References

[1] Feldmann, H., Volchkov, V.E., Volchkova, V.A. and Klenk, H.D. (1999) in: 100 Years of Virology (Calisher, C.H. and Horzinek, M.C., Eds.), pp. 159–169, Springer-Verlag, Vienna.
[2] Volchkov, V.E. (1999) Curr. Top. Microbiol. Immunol. 235, 35–47.
[3] Weissenhorn, W., Carfi, A., Lee, K., Skehel, J.J. and Wiley, D.C. (1998) Mol. Cell 2, 605–616.
[4] Malashkevich, V.N., Schneider, B.J., McNally, M.N., Milhollen, M.A., Pang, J.X. and Kim, P.S. (1999) Proc. Natl. Acad. Sci. USA 96, 2662–2667.
[5] Watanabe, S., Takada, A., Watanabe, T., Ito, H., Kida, H. and Kawaoka, Y. (2000) J. Virol. 74, 10194–10201.
[6] Bavari, S., Bosio, C.M., Wiegand, E., Ruthel, G., Will, A.B., Geisbert, T.W., Hevey, M., Schmaljohn, C., Schmaljohn, A. and Javad Aman, M. (2002) J. Exp. Med. 195, 593–602.
[7] Gallaher, W.R. (1996) Cell 85, 477–478.
[8] Ruiz-Argüello, M.B., Goñi, F.M., Pereira, F.B. and Nieva, J.L. (1998) J. Virol. 72, 1775–1781.
[9] Ito, H., Watanabe, S., Sánchez, A., Whitt, M.A. and Kawaoka, Y. (1999) J. Virol. 73, 8907–8912.
[10] White, S.H. and Wimley, W.C. (1999) Annu. Rev. Biophys. Biomol. Struct. 28, 319–365.
[11] Suárez, T., Gallaher, W.R., Agirre, A., Goñi, F.M. and Nieva, J.L. (2000) J. Virol. 74, 8038–8047.
[12] Wimley, W.C. and White, S.H. (1996) Nat. Struct. Biol. 3, 842–848.
[13] Eisenberg, D., Weiss, R.M. and Terwilliger, T.C. (1982) Nature 299, 371–374.
[14] Eisenberg, D., Weiss, R.M. and Terwilliger, T.C. (1984) Proc. Natl. Acad. Sci. USA 81, 140–144.
[15] Hope, M.J., Bally, M.B., Webb, G. and Cullis, P.R. (1985) Biochim. Biophys. Acta 812, 55–65.
[16] Böttcher, C.S.F., van Gent, C.M. and Fries, C. (1961) Anal. Chim. Acta 24, 203–204.
[17] Maget-Dana, R. (1999) Biochim. Biophys. Acta 1462, 109–140.

[18] White, S., Wimley, W.C., Ladokhin, A.S. and Hristova, K. (1998) Methods Enzymol. 295, 62–87.
[19] Ellens, H., Bentz, J. and Szoka, F.C. (1985) Biochemistry 24, 3099–3106.
[20] Nieva, J.L., Nir, S., Muga, A., Goñi, F.M. and Wilschut, J. (1994) Biochemistry 33, 3201–3209.
[21] Arrondo, J.L.R. and Goñi, F.M. (1999) Prog. Biophys. Mol. Biol. 72, 367–405.
[22] White, S.H., Ladokhin, A.S., Jayasinghe, S. and Hristova, K. (2001) J. Biol. Chem. 276, 32395–32398.
[23] Ladokhin, A.S. and White, S.H. (1999) J. Mol. Biol. 285, 1363–1369.
[24] Ladokhin, A.S. and White, S.H. (2001) J. Mol. Biol. 309, 543–552.
[25] Marsh, D. (1996) Biochim. Biophys. Acta 1286, 183–223.
[26] Rietveld, A. and Simons, K. (1998) Biochim. Biophys. Acta 1376, 467–479.
[27] Brown, D.A. and London, E. (2000) J. Biol. Chem. 275, 17221–17224.
[28] Veiga, M.P., Goñi, F.M., Alonso, A. and Marsh, D. (2000) Biochemistry 39, 9876–9883.
[29] Benachir, T. and Lafleur, M. (1995) Biochim. Biophys. Acta 1235, 452–460.
[30] Ladokhin, A.S., Selsted, M.E. and White, S.H. (1997) Biophys. J. 72, 1762–1766.
[31] Ladokhin, A.S. and White, S.H. (2001) Biochim. Biophys. Acta 1514, 253–260.
[32] Hristova, K., Dempsey, S.H. and White, S.H. (2001) Biophys. J. 80, 801–811.
[33] Pott, T., Paternostre, M. and Dufourc, E.J. (1998) Eur. Biophys. J. 27, 237–245.
[34] Sáez-Cirión, A., Nir, S., Lorizate, M., Agirre, A., Cruz, A., Pérez-Gil, J. and Nieva, J.L. (2002) J. Biol. Chem. 277, 21776–21785.
[35] Zwick, M.B., Labrijn, A.F., Wang, M., Spenlehauer, C., Ollmann, E., Binley, J.M., Moore, J.P., Stiegler, C., Katinger, H., Burton, D.R. and Parren, P.W.H.I. (2001) J. Virol. 75, 10892–10905.